

Modeling and assimilation of root zone soil moisture using remote sensing observations in Walnut Gulch Watershed during SMEX04

N.N. Das^a, B.P. Mohanty^{a,*}, M.H. Cosh^b, T.J. Jackson^b

^a Department of Biological and Agricultural Engineering, Texas A&M University, College Station, Texas 77843-2117, United States

^b USDA ARS Hydrology and Remote Sensing Lab, Beltsville, MD 20705, United States

Received 19 April 2006; received in revised form 6 October 2006; accepted 26 October 2006

Abstract

Soil moisture status in the root zone is an important component of the water cycle at all spatial scales (*e.g.*, point, field, catchment, watershed, and region). In this study, the spatio-temporal evolution of root zone soil moisture of the Walnut Gulch Experimental Watershed (WGEW) in Arizona was investigated during the Soil Moisture Experiment 2004 (SMEX04). Root zone soil moisture was estimated *via* assimilation of aircraft-based remotely sensed surface soil moisture into a distributed Soil–Water–Atmosphere–Plant (SWAP) model. An ensemble square root filter (EnSRF) based on a Kalman filtering scheme was used for assimilating the aircraft-based soil moisture observations at a spatial resolution of 800 m × 800 m. The SWAP model inputs were derived from the SSURGO soil database, LAI (Leaf Area Index) data from SMEX04 database, and data from meteorological stations/rain gauges at the WGEW. Model predictions are presented in terms of temporal evolution of soil moisture probability density function at various depths across the WGEW. The assimilation of the remotely sensed surface soil moisture observations had limited influence on the profile soil moisture. More specifically, root zone soil moisture depended mostly on the soil type. Modeled soil moisture profile estimates were compared to field measurements made periodically during the experiment at the ground based soil moisture stations in the watershed. Comparisons showed that the ground-based soil moisture observations at various depths were within ±1 standard deviation of the modeled profile soil moisture. Density plots of root zone soil moisture at various depths in the WGEW exhibited multi-modal variations due to the uneven distribution of precipitation and the heterogeneity of soil types and soil layers across the watershed.

© 2007 Elsevier Inc. All rights reserved.

Keywords: SMEX04; Root zone soil moisture; Data assimilation; Soil properties

1. Introduction

Surface and root zone soil moisture are important state variables for hydrological and meteorological modeling. The sensitivity of energy exchange processes at the land–atmosphere boundary to root zone soil moisture is well known. These processes are important for global water circulation and carbon cycling. Passive microwave remote sensing has the potential to provide synoptic surface soil moisture measurements (Engman & Gurney, 1991; Jackson, 1993; Jackson et al., 1999; Njoku & Entekhabi, 1995) that are important for assessment of root zone soil moisture over a region. These measurements describe near-surface (0–0.05 m) soil moisture

(Jackson & Schmugge, 1989; Schmugge et al., 1974, 1977, 1980). Recognizing the importance of surface and root zone soil moistures, major efforts are underway to develop operational soil moisture remote sensing techniques. Scientific campaigns such as Washita 1992, Southern Great Plains hydrology experiments 1997 (SGP97), and Soil Moisture Experiments 2004 (SMEX04) were conducted to validate airborne and spaceborne passive microwave remote sensing platforms and thus estimating soil moisture over large spatial scales. These campaigns were conducted in selected geographical regions representing rangeland, agricultural farmland, and semi-arid shrubland, as well as different topographic conditions such as flat, rolling/undulating, and mountainous terrains.

Kostov and Jackson (1993), and Wei (1995) suggested that a promising approach for estimating profile soil moisture is the integration of remote sensing surface soil moisture data and

* Corresponding author. Tel.: +1 979 458 4421.

E-mail address: bmohanty@tamu.edu (B.P. Mohanty).

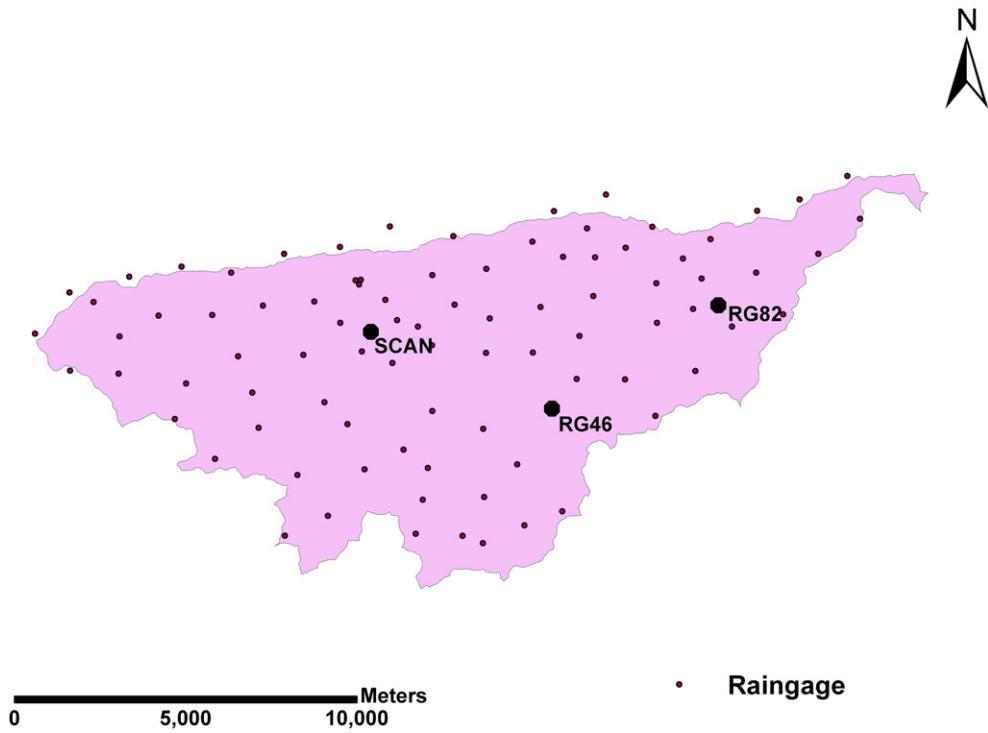


Fig. 1. Walnut Gulch Experimental Watershed (WGEW) with rain gages, SCAN, RG46, and RG82 sites used in the study.

computational modeling. In the case of bare soil, Entekhabi et al. (1994) showed that it is possible to retrieve profile soil water content using passive microwave data at frequencies less than 10 GHz. In that study, the propagation of information from

the surface to deeper soil layers was investigated using a multilayer model of heat and water transfer. Houser et al. (1998) studied the use of four-dimensional data assimilation methods in a macro-scale land hydrology model to generate surface and

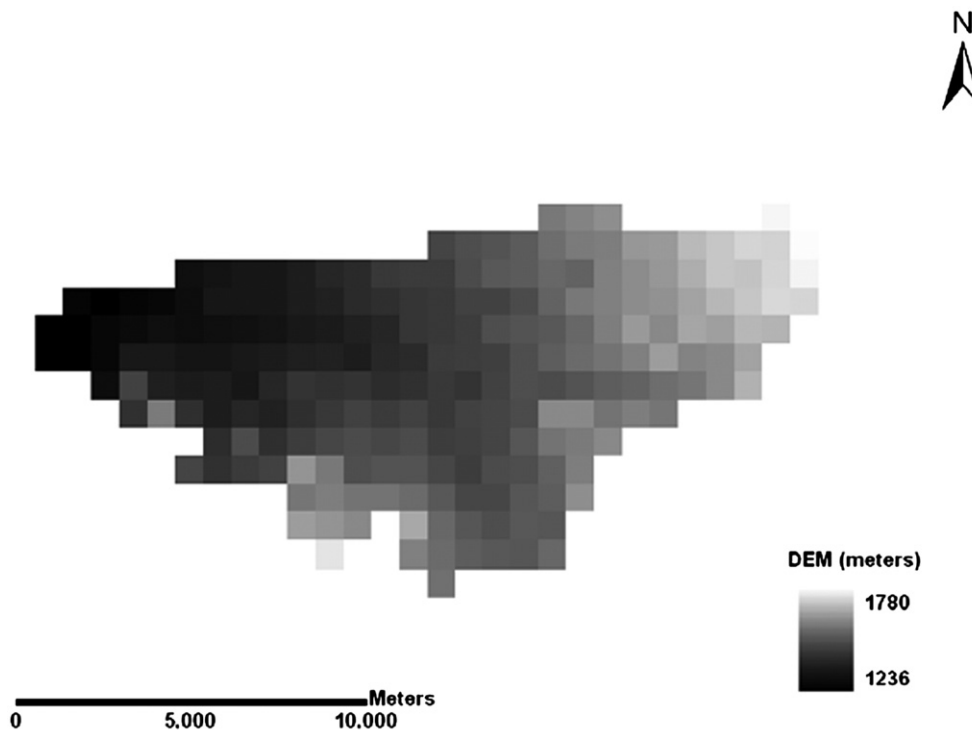


Fig. 2. Walnut Gulch Experimental Watershed (WGEW) digital elevation model (DEM) at resolution of 800 m × 800 m, resampled from 30 m × 30 m DEM. Data source: USDA geospatial-data-gateway.

root zone soil moisture fields at regular space and time intervals for the Walnut Gulch Experimental Watershed (WGEW) in Arizona. Other related/similar studies have been conducted for estimation of surface and profile soil water contents using passive microwave data at watershed/regional scale during the SGP97 experiment (e.g., Crosson et al., 2002; Crow & Wood, 2003; Das & Mohanty, 2006; Dunne & Entekhabi, 2005; Margulis et al., 2002; Reichle et al., 2002).

The primary objective of this study is to determine the evolution of the spatial and temporal dynamics of root zone soil moisture in semi-arid shrublands of the WGEW during the SMEX04 experiment. We have used an Ensemble Square Root Filter (EnSRF) to assimilate aircraft-based (Polarimetric Scanning Radiometer) remotely sensed surface soil moisture observations with the Soil–Water–Atmosphere–Plant (SWAP) model for the estimation of profile soil water content. The assimilation of Polarimetric Scanning Radiometer (PSR/CX)-based surface soil moisture and modeling of root zone soil moisture were conducted by extending the parallel non-interacting stream tube framework proposed by Das and Mohanty (2006) and also included run-off and run-on processes between remote sensing footprints. The temporal evolution of soil moisture measured at point-based monitoring locations and depths across the WGEW was also compared with EnSRF-based model predictions. A secondary objective of this study is to develop the probability distributions for soil moisture at various depths within the WGEW.

2. Materials and methods

2.1. Description of study area and forcings

The SMEX04 field campaign was conducted between August 2 and August 27, 2004 across Arizona, USA and Sonora, Mexico (<http://hydrolab.arsusda.gov/smex04/>). The primary focus of the field experiments in Arizona during SMEX04 was the Walnut Gulch Experimental Watershed (31°43'N, 110°41'W) near Tombstone, operated by the Agriculture Research Service (ARS), U.S. Department of Agriculture (USDA). The 150 km² watershed (Fig. 1) is part of the San Pedro river basin, and is heavily instrumented to measure rainfall and runoff. The instrumented area of the watershed comprises a dense network of 88 rain-gages (Fig. 1) of which 19 are collocated with soil moisture sensors. The elevation of the WGEW (Fig. 2) varies between 1250 m and 1585 m above the mean sea level, with an average annual temperature of 17.7 °C. It receives an average of 350 mm of precipitation annually. The vegetation is mainly shrubs, covering about two-thirds of the watershed. The remaining one-third is mostly grassland. The soil is generally well drained, calcareous, gravelly loam with large percentages of rock and gravel at the soil surface. Natural Resources Conservation Services (NRCS) has mapped 27 soil series in this watershed. The soil classification based on dominant surface soil texture at a resolution of 800 m × 800 m is illustrated in Fig. 3. Complete information about the WGEW is available on

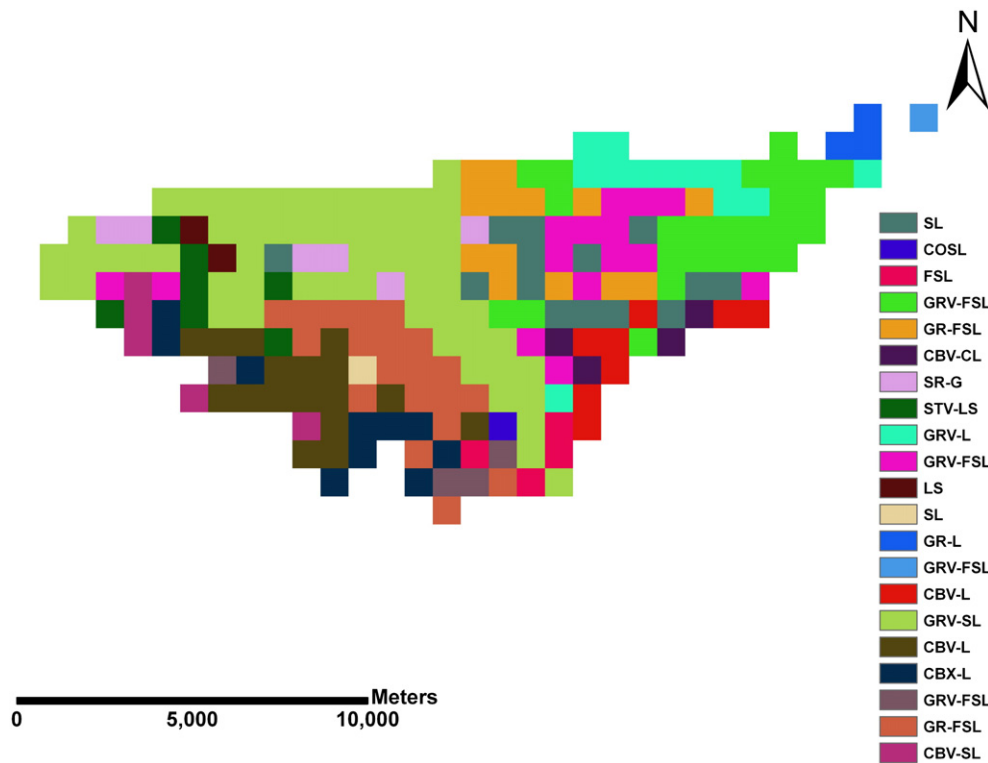


Fig. 3. Walnut Gulch Experimental Watershed (WGEW) surface soil texture at resolution 800 m × 800 m (SL: sandy loam; COSL: coarse sandy loam; FSL: fine sandy loam; GRV-FSL: very gravelly fine sandy loam; GR-FSL: gravelly fine sandy loam; CBV-CL: very cobbly clay loam; SR-G: stratified gravel; STV-LS: very stony loamy sand; GRV-L: very gravelly loam; LS: loamy sand; GR-L: gravelly loam; CBV-L: very cobbly loam; GRV-SL: very gravelly sandy loam; CBX-L: extremely cobbly loam; CBV-SL: very cobbly sandy loam). Data source: <http://soildatamart.nrcs.usda.gov/County.aspx?State=AZ>.

the USDA-ARS website (<http://ars.usda.gov/SP2UserFiles/Place/53424500/WGBrochure.pdf>). During SMEX04 campaign, the PSR/CX (Piepmeier & Gasiewski, 2001) with polarimetric channels of C and X band (5.82–10.80 GHz) was flown on the Naval Research Lab's (NRL) P3 aircraft. The P3 flight details of the remote sensing campaign are available at National Snow and Ice Data Center (NSIDC). The PSR/CX-based soil moisture snapshots for 9 days across the WGEW are illustrated in Fig. 4 (Bindlish et al., 2008-this issue).

The footprint size (800 m × 800 m) of PSR/CX was used as the basis for grid resampling (by inverse-distance interpolation) for all variables resulting in a total of 224 pixels across the WGEW. The resulting daily spatially distributed hydro-climatic datasets were used as inputs to the SWAP model. For this distributed modeling and data assimilation study, we used input data from various sources including the LAI data collected during SMEX04 campaign, the soil layers and types from the SSURGO database (USDA-NRCS), and the precipitation data collected by the network of 88 weighing-type recording rain-gages arranged in a grid across the WGEW (Fig. 1). An inverse-distance interpolation (IDI) technique was used to create a spatial distribution of daily accumulated precipitation on relevant dates (Fig. 5). It is apparent from Fig. 5 that during the SMEX04 period WGEW received scattered and scanty rainfall with no major precipitation event throughout the watershed. The spatial distribution of LAI (800 m × 800 m) across WGEW was also generated with IDI technique (Fig. 6). All other meteorological forcings (e.g., relative humidity, wind

speed, and air temperature) were extracted from the Soil Climate Analysis Network (SCAN) site located within WGEW (Fig. 1), and were assumed to be spatially uniform for the purpose of this study. The relevant GIS and ground measurement datasets available at NSIDC were used for distributed modeling of root zone soil moisture in the WGEW.

2.2. Soil–Water–Atmosphere–Plant (SWAP) model

SWAP (Van Dam et al., 1997) is a robust physically-based field scale eco-hydrological model used to simulate the processes occurring in the soil–water–atmosphere–plant system. SWAP is an open source hydrological model and is the successor of the SWATR model (Feddes et al., 1978). SWAP is available at <http://www.swap.alterra.nl/>. The model simulates both the soil water quantity and quality with daily temporal resolution. SWAP can account for several combinations of the top and bottom boundary conditions. Ines and Honda (2005) have successfully used SWAP in their study for quantifying surface and root zone soil water contents from low resolution remote sensing data. Since SWAP was not originally designed for distributed modeling, it was adapted into a framework developed by Das and Mohanty (2006). This framework was developed on ArcGIS platform for distributed hydrological modeling. It uses geophysical variables in grid format as inputs to the hydrologic model (SWAP). The framework is capable of producing soil moisture outputs at watershed-scale at various depths in a grid format. For this study, run-on and run-off

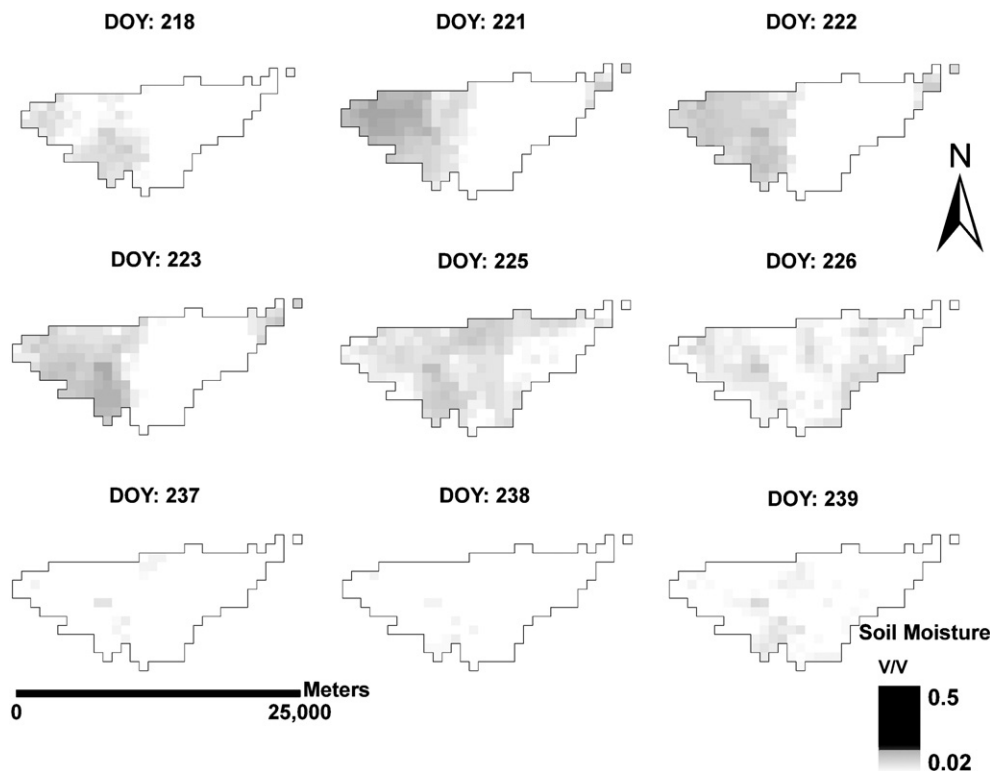


Fig. 4. Walnut Gulch Experimental Watershed (WGEW) PSR/CX snapshots of soil moisture for Day of Year (DOY) 218, 221, 222, 223, 225, 226, 237, 238, and 239 at resolution of 800 m × 800 m.

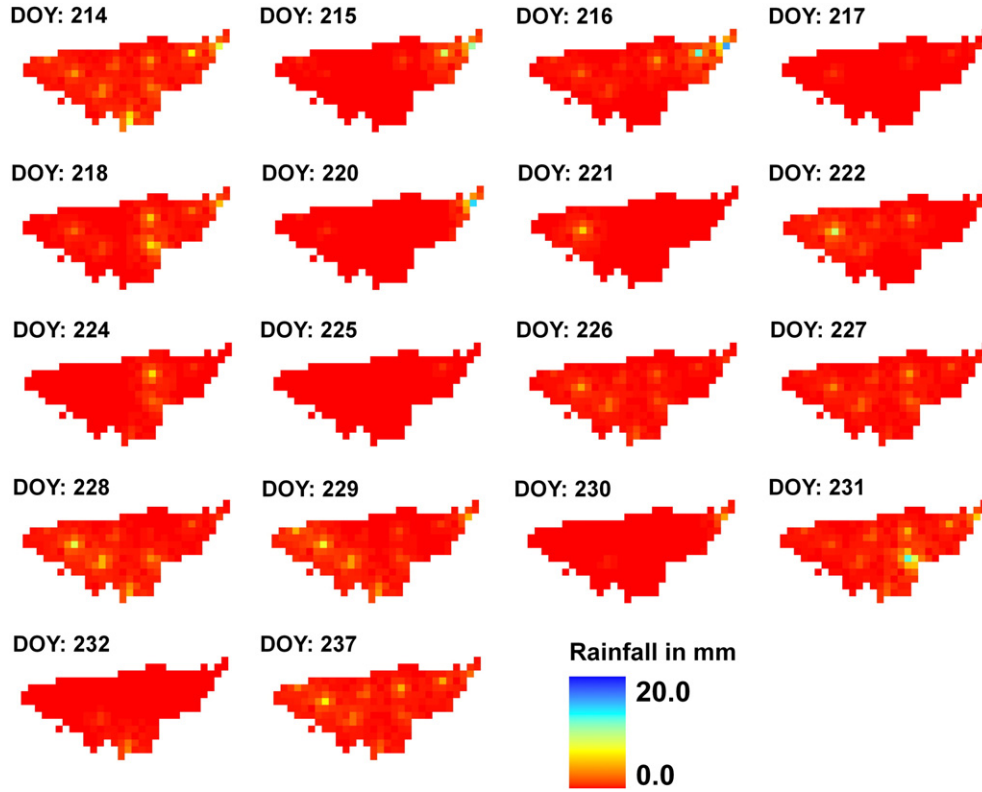


Fig. 5. Spatial distribution of precipitation at resolution of 800 m × 800 m created with inverse distance interpolation (IDI) of measurements from 88 raingages in Walnut Gulch Experimental Watershed (WGEW).

routing were also included in the framework by extracting flow-accumulation, flow-direction, and flow-length information from the digital elevation model (DEM) (Fig. 2) of the WGEW with a steepest descent technique. Note, however, the DEM of 800 m × 800 m resolution (resampled from 30 m × 30 m resolution) may introduce some scale uncertainty while evaluating flow-accumulation, flow-direction, and flow length.

The governing equation of SWAP solves the 1-D Richards' equation (Eq. (1)) to simulate partially-saturated water movement in the soil profile.

$$\frac{\partial \theta}{\partial t} = \frac{\partial}{\partial z} \left[K \left(\frac{\partial h}{\partial z} + 1 \right) \right] - S_a(h) \quad (1)$$

where θ is the soil water content (m^3/m^3), z is the soil depth (m), h is the soil water pressure head (m), K is the unsaturated hydraulic conductivity (m/day), and $S_a(h)$ is the root water uptake (m/day). The maximum possible root water uptake over the rooting depth is equal to potential transpiration rate, T_p (m/day), which is governed by atmospheric conditions. The potential root water uptake at a certain depth, $S_p(z)$, may be determined by the root length density, $l_{root}(z)$ (m/m^3), as a fraction of the integrated root length density.

$$S_p(z) = \frac{l_{root}(z)}{\int_0^{D_{root}} l_{root}(z) dz} T_p \quad (2)$$

where D_{root} is the root layer thickness. In practice the distribution of $l_{root}(z)$ is often not available. Therefore in SWAP, a uniform root length density distribution is assumed.

$$\frac{l_{root}(z)}{\int_0^{D_{root}} l_{root}(z) dz} = \frac{1}{D_{root}} \quad (3)$$

which leads to the simplification of Eq. (2) (Feddes et al., 1978), as

$$S_p(z) = \frac{T_p}{D_{root}} \quad (4)$$

The actual root water uptake $S_a(h)$, is calculated from

$$S_a(h) = \alpha_w \int_0^{D_{root}} S_p(z) dz \quad (5)$$

α_w is the reduction factor as a function of h that accounts for water stress (Feddes et al., 1978). Penman–Monteith equation (Monteith, 1965) was used to calculate potential evapotranspiration. The potential transpiration (T_p) and the soil evaporation (E_p) were partitioned using LAI. The potential evaporation rate of soil under standing vegetation is derived from Penman–Monteith equation by neglecting the aerodynamic term. Thus, the only source of soil evaporation is net radiation that reaches

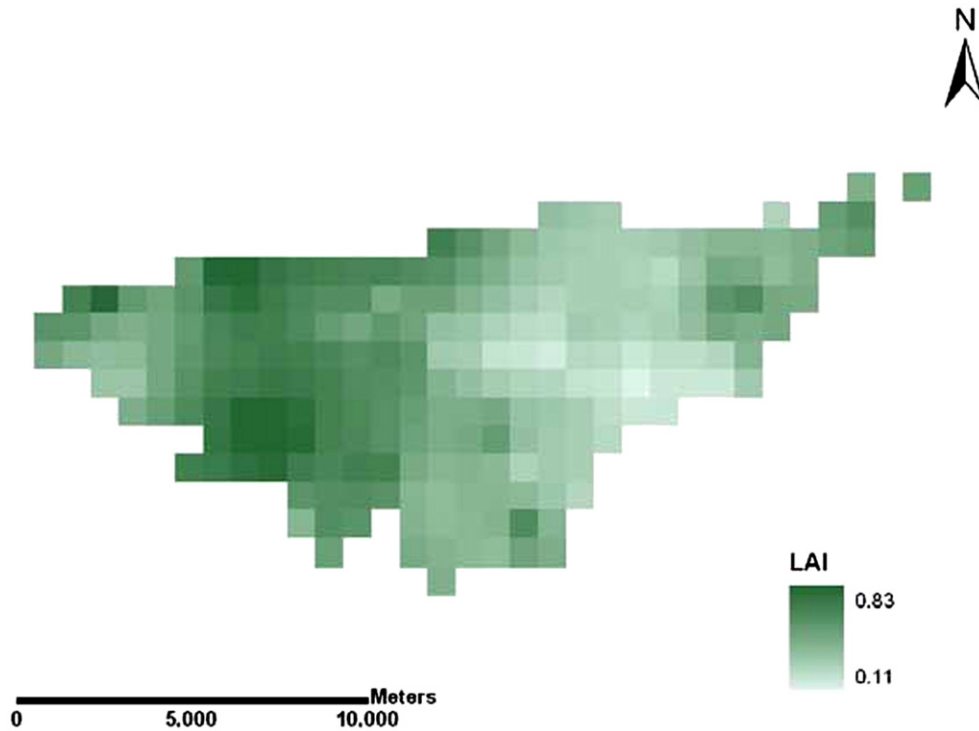


Fig. 6. Walnut Gulch Experimental Watershed (WGEW) Leaf Area Index (LAI) at resolution of $800 \text{ m} \times 800 \text{ m}$. Data source: http://nsidc.org/data/amsr_validation/soil_moisture/smex04/.

the soil surface. Assuming that the net radiation inside the canopy decreases according to an exponential function, we can derive

$$E_p = E_{po} e^{-\kappa_{gr} \text{LAI}} \quad (6)$$

where κ_{gr} is the extinction coefficient of global solar radiation and E_{po} (m/day) is potential evaporation. SWAP calculates the daily average T_p (m/day),:

$$T_p = (1.0 - W_{\text{frac}}) E_{T_{po}} - E_p \quad (7)$$

where W_{frac} (-) is ratio of the daily amount of intercepted precipitation and potential evaporation rate of the water intercepted by the vegetation. In Eq. (7) $E_{T_{po}}$ (m/day) is potential evapotranspiration rate of a dry canopy.

In the SWAP model soil moisture retention and hydraulic conductivity functions are defined by the Mualem–van Genuchten equation,

$$S_e = \frac{\theta(h) - \theta_r}{\theta_s - \theta_r} = \left[\frac{1}{1 + |\alpha h|^n} \right]^m \quad (8)$$

$$K(S_e) = K_0 S_e^1 \{1 - [1 - S_e^{n/(n-1)}]^{1-1/n}\}^2 \quad (9)$$

where S_e is the relative saturation (-), θ_s and θ_r are the saturated and residual water content (m^3/m^3) respectively, α (m^{-1}), n (-), m (-) are the shape parameters of the soil water retention function and $m = 1 - 1/n$, K_0 is the matching point at saturation (m/s), and parameter l (-) is an empirical pore tortuosity/connectivity parameter.

2.2.1. SWAP modeling domain and parameters

The spatially and temporally variable atmospheric forcings, soil hydraulic properties, and vegetation interact in a highly nonlinear manner to produce heterogeneous soil moisture at the soil surface and in the root zone. In this paper, we mainly focused on watershed-scale representations of the root zone soil moisture at a coarser spatial resolution of $800 \text{ m} \times 800 \text{ m}$ and temporal resolution of one day. Therefore, the disparity of scales between the horizontal (spatial resolution: $800 \text{ m} \times 800 \text{ m}$) and vertical (soil depth: 3.86 m) extents of the root zone was the key consideration in formulating the framework for watershed-scale root zone hydrology. For SWAP model simulation, the 3.86 m thick soil profile (available soil depth in SURRGO database) at every remote sensing footprint was discretized into 50 nodes, with finer discretization near the soil layer interfaces and at the land–atmosphere boundary. Finer discretization near the top boundary and layer interfaces were used to handle the steep pressure gradient for the numerical simulations. Time-dependent flux-type top boundary conditions for each parallel soil column (matching the remote sensing footprints) were used with precipitation distribution across the WGEW. A unit vertical hydraulic gradient (free drainage) condition was used at the bottom boundary of the soil columns because of deep groundwater table (45 m to 150 m) condition across the WGEW. No flow bottom boundary condition was imposed where impervious layers (*i.e.*, bedrocks) were encountered in 3.86 m of the soil profile. Runoff and runoff between adjacent footprints due to topography was considered on the land surface. The runoff from the one or more adjacent pixels of steepest descent according to flow routing was used as runoff for

the pixel under consideration. Given the relatively coarse horizontal scale with shallow root zone, the parallel soil columns model ignores the lateral water fluxes across the adjacent soil columns and only predicts the vertical fluxes including infiltration, evapotranspiration, runoff, and deep percolation as parallel non-interacting stream-tubes concept in distributed vadose zone hydrology. We also assumed that 1-D Richards' equation is an appropriate physical model to simulate vertical partially-saturated flow and partitioning of fluxes at the spatial scale of 800 m × 800 m. Numerical studies conducted by Mantoglou (1992), and Zhang (1999) on general upscaled Richards' equations have shown that at large spatial scales and in the absence of interflow vadose zone flow can be represented by one-dimensional Richards' equation.

A probabilistic approach was adopted in the distributed modeling environment across the WGEW. An ensemble of state variables (profile soil moistures) was created for all the 224 (800 m × 800 m) PSR/CX footprints in the WGEW. A state augmentation technique was applied by concatenating uncertain soil properties to state variables, forming composite vectors in the ensemble. The soil hydraulic properties (θ_s , θ_r , and K_{sat}) from the SSURGO database were used to introduce uncertainty in the ensemble. The van-Genuchten shape parameters (α , and n) for the soil textural classes given by Carsel and Parrish (1988) were used with $\pm 20\%$ uncertainty. The purpose of including uncertain soil properties in the ensemble is to address the assumption that it simulates model errors and subpixel variability present within a PSR/CX footprint.

For best computational efficiency, one hundred members (composite vectors) were populated in the ensemble. The soil moisture in the discretized soil profile was assigned an initial value of 50% relative saturation according to the soil texture on the onset of model simulation. A Gaussian noise of 20% to 5% of the initial soil moisture (in decreasing order from top to bottom of the soil profile) was introduced in all the ensemble members with an assumption of decreasing variability in soil moisture with increasing depth. The SWAP model was run a month ahead of the SMEX04 campaign (August 2nd, 2004 through August 27th, 2004), to tune the state of initial soil moisture profile. PSR/CX-measured surface soil moisture was assimilated with the SWAP model predictions (across the 3.86 m of soil layer) through the ensemble square root filter (EnSRF) updating scheme described below. At each time step, final states were determined by averaging the ensemble of the one hundred replicated predictions made by the model.

2.3. Ensemble Square Root Filter (EnSRF)

An enduring problem in many hydrologic situations is to forecast the state of a system given a set of observations and a hydrologic model. While the use of deterministic models has significantly addressed this problem, it now appears that much more promising solutions lie with probabilistic forecasting and data assimilation. In hydrology, the ensemble Kalman filters (EnKF; Evensen, 2003; Houtekamer & Mitchell, 1998) based on the Monte-Carlo approach are generally used (e.g., Crosson et al., 2002; Crow & Wood, 2003; Das & Mohanty, 2006;

Dunne & Entekhabi, 2005; Margulis et al., 2002; Reichle et al., 2002). Use of the Kalman filter system implicitly assumes that the observations are related to the true state x^t through

$$y = Hx^t + \varepsilon \quad (10)$$

where ε is a Gaussian random error vector with a mean of zero and measurement error covariance R , and H is the operator that maps the model variable space to the observation space. Furthermore, the forecast of x_t is Gaussian with mean $x_{t=k}^f$ and error covariance $P_{t=k}^f$. Using these assumptions, the estimated state of the profile soil moisture and error covariance is updated as

$$x_{t=k}^a = x_{t=k}^f + K(y - Hx_{t=k}^f) \quad \text{and} \quad (11)$$

$$P_{t=k}^a = (I - KH)P_{t=k}^f. \quad (12)$$

Here, the superscripts f and a represent the respective prior (forecast) and posterior (analysis/updated) estimates, the subscript t represents time, y is the observation vector, I is the identity matrix, and K is the Kalman gain matrix defined as:

$$K = P_{t=k}^f H^T (HP_{t=k}^f H^T + R)^{-1} \quad (13)$$

The EnKF forecast and analysis error covariance comes directly from an ensemble of model simulations as:

$$P^f H^T = (N_e - 1)^{-1} \sum_{n=1}^{N_e} (x_n^f - \bar{x}^f)(Hx_n^f - H\bar{x}^f)^T \quad (14)$$

N_e is the number of ensemble members, and the subscript n represents each individual ensemble member. The overbar represents the ensemble mean, which is sampled as

$$\bar{x}^f = N_e^{-1} \sum_{n=1}^{N_e} x_n^f \quad (15)$$

The ensemble is generated by perturbing a first-guess value so that ensemble mean is equal to the first-guess value. The variance is specified based on the uncertainty in the first-guess. In this system, ensemble members are integrated independently and updated in accordance with the Kalman filter methods when new observations become available.

An alternate version of the EnKF approach is required in our study to ensure that the analysis error covariance does not become unrealistically low. Burgers et al. (1998) demonstrated that P^a is underestimated by a factor of $I - KH$ when observations are not treated as random variables. This can cause the EnKF to reject observations in favor of the ensemble forecast. This leads the analysis incrementally further away from reality, resulting in filter divergence (e.g., Burgers et al. 1998; Houtekamer & Mitchell 1998; Mitchell & Houtekamer 2000; Whitaker & Hamill 2002). Whitaker and Hamill (2002) showed that adding random noise to observations further skews the distribution of P^a , and this results in a more erroneous

analysis even though the covariance is increased. They suggested an alternative ensemble square root filter (EnSRF) where the ensemble mean is still updated by Eq. (11), but deviations from the mean are updated by

$$x_{t=k}^a = x_{t=k}^f + K'(Hx_{t=k}^f) \quad (16)$$

where

$$K' = \alpha K \quad (17)$$

and

$$\alpha = 1 + \sqrt{\frac{R}{HPH + R}} \quad (18)$$

Using this method, the analysis error covariance is guaranteed to be exactly equal to that in Eq. (11), and perturbed observations are no longer necessary ($y^f=0$). This scalar version of EnKF for the assimilation of a single observation at a time was implemented in this study.

3. Results and discussion

3.1. Modeling and verification

The model run for the period of SMEX04 resulted in soil moisture estimation up to a profile depth of 3.86 m in all 224 pixels of the WGEW. Fig. 7 illustrates the evolution of average (from pixel ensemble) soil moisture fields at the depths of 0.05, 0.20, 1.00, and 3.50 m for August 8th, 2004 (Day of Year, DOY, 221). To evaluate the model performance, model outputs were compared with soil moisture observations from the SCAN and

Hydra sites (RG46 and RG82) at WGEW (highlighted in Fig. 1). The modeled footprint-scale profile soil moisture at a particular depth was compared with the corresponding local (point-scale) profile soil moisture data measured at these three sites. It is suggested that the ensemble variability of soil moisture within a pixel (800 m × 800 m) reflects the variability at the subpixel/point scale at the respective depth. The evolution of profile soil moisture states at corresponding footprint-scale and local/point-scale were greatly influenced by the soil layers, antecedent moisture conditions, soil hydraulic properties, and precipitation (Fig. 8). Table 1 shows the layer depth (z), saturated hydraulic conductivity (K_{sat}), residual water content (θ_r), saturated water content (θ_s), and soil texture for various soil layers (from SSURGO database) up to 3.86 m depth at the SCAN and Hydra sites representing typical conditions of the WGEW. The following discussion elaborates the comparisons of modeled and observed profile soil moisture values at these three sites.

3.1.1. SCAN site

The SCAN site is a semiarid shrubland located at an altitude of 1362 m above the sea level. The SCAN site is typical of WGEW with very gravelly sandy soil texture and high saturated hydraulic conductivity (Table 1). The site has 5 distinct soil layers up to the depth of 3.86 m. The top 4 layers at the site have similar K_{sat} , but dissimilar θ_r and θ_s due to different degrees of compaction. The SCAN site observations at the depths of 0.05, 0.10, 0.20, 0.50 and 1.00 m are plotted in Fig. 9a–e. Model prediction with PSR/CX-based data assimilation and open-loop (model prediction without data assimilation) are also plotted in these figures. The subpixel variability in the PSR/CX-assimilated prediction is shown as ± 1 standard deviation (SD) in the plots. From Fig. 9a, it is clear that at

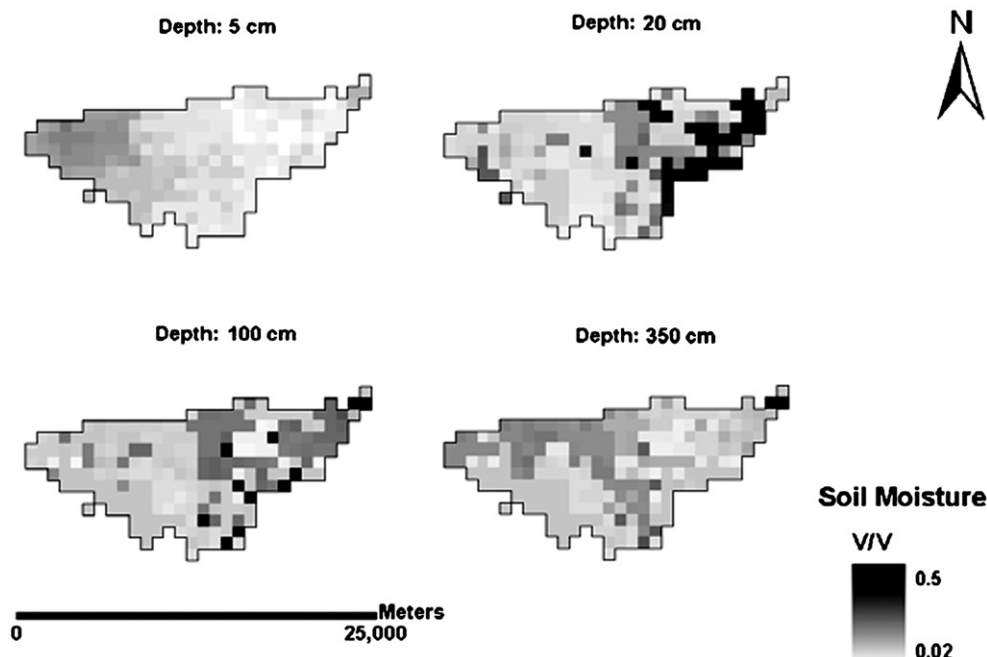


Fig. 7. Walnut Gulch Experimental Watershed (WGEW) model (with assimilation) simulated soil moisture for Day of Year (DOY) 219 at depth 0.05 m, 0.20 m, 1.00 m, and 3.50 m at resolution of 800 m × 800 m.

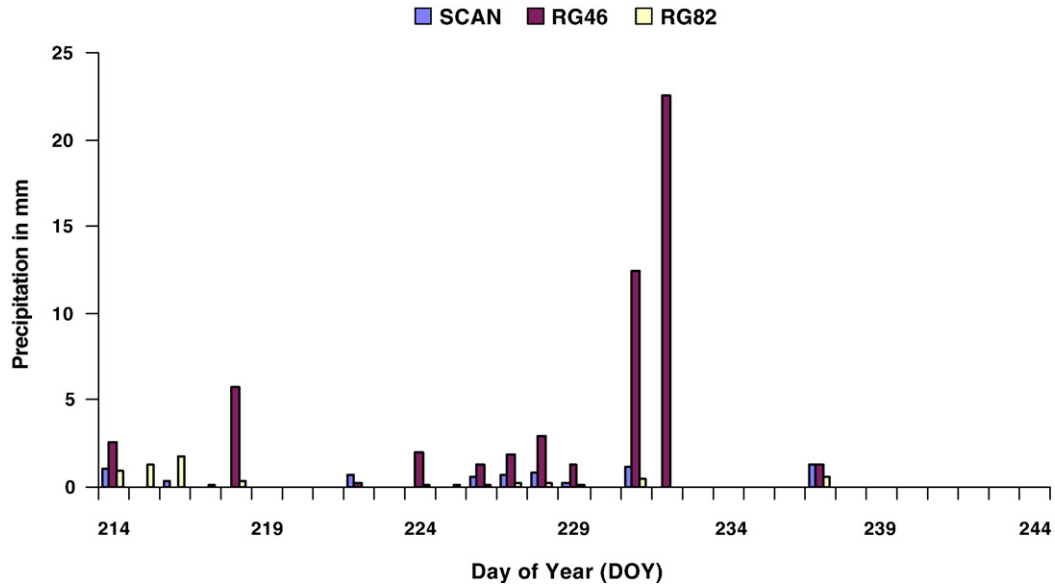


Fig. 8. Precipitation in mm observed in three sites (SCAN, RG46 and RG82).

0.05 m depth, SCAN observations and PSR/CX observations disagree for the initial study period. During the initial dry days (DOY: 214–220) the model predictions (with and without data assimilation) were close to θ_r (0.039 based on SSURGO), whereas SCAN observations are much below this value and were beyond the ± 1 SD. One explanation for such low SCAN observations is the presence of rock and gravel fraction in the top 0.13 m of soil depth. High rock and gravel fraction influence the soil hydraulic characteristics making them highly nonlinear with very high saturated hydraulic conductivity, which drains the soil rapidly. The other reason for the discrepancy between the SCAN point-scale (observation) and PSR pixel-scale (modeled) soil moisture is that the SCAN site received scanty rainfall during SMEX04 (Fig. 8). In dry conditions the model was constrained due to the lower limit set by θ_r (from SSURGO dataset). Thus, on DOY 219, assimilating PSR/CX observations made the model prediction deviate further away from the SCAN observations (Fig. 9a). During the rest of the SMEX04 experiment (DOY: 222

to 244), with the increase in soil moisture at 0.05 m depth, the model prediction trend matches reasonably well with the SCAN observations. At the depths of 0.10, 0.20, and 0.50 m (Fig. 9b–d) the SCAN observations are close to ± 1 SD of the model predictions with data assimilation using PSR-based data. The deepest SCAN site observations at 1.00 m depth show a uniform state of soil moisture and the trend matches with both the models (assimilated and open-loop), and are also contained completely within ± 1 SD of assimilated model predictions. Most SCAN observations lie within ± 1 SD of the assimilated model predictions. This provides some evidence that the spatial variability is well represented by the model ensemble for the particular pixel. The open-loop model also performed somewhat similar to the assimilated model at the deeper depths (Fig. 9b–e), demonstrating the dominant effect of soil texture in the evolution of soil moisture distribution at the deeper depths, irrespective of the model. Fig. 9a–e also show that the propagation of EnSRF Kalman gain through the land surface model reaches deeper with

Table 1

Saturated hydraulic conductivity, water content (residual and saturated), and soil texture of various soil layers at the SCAN site and the Hydra sites of Walnut Gulch Experimental Watershed (WGEW)

| Site | Soil layers depth (m) | | K_{sat} (m/day) | | | Water content (%) | | Soil texture description |
|--------------|-----------------------|--------|-------------------|------|------|-------------------|-----------|--------------------------|
| | Top | Bottom | Min. | Avg. | Max. | Residual | Saturated | |
| SCAN | 0 | 0.127 | 1.20 | 2.41 | 3.62 | 3.9 | 25 | Very gravelly sandy loam |
| | 0.127 | 0.83 | 1.20 | 2.41 | 3.62 | 5.7 | 33 | Gravelly sandy loam |
| | 0.83 | 2.00 | 1.20 | 2.41 | 3.62 | 6.6 | 40 | Sandy loam |
| | 2.00 | 251.46 | 1.20 | 2.41 | 3.62 | 5.5 | 33 | Gravelly sandy loam |
| | 2.51 | 3.86 | 0.34 | 0.77 | 1.20 | 6.1 | 37 | Gravelly loam |
| RG46 (Hydra) | 0 | 0.07 | 1.20 | 2.41 | 3.62 | 8 | 41 | Fine sandy loam |
| | 0.07 | 0.45 | 0.12 | 0.23 | 0.34 | 17.5 | 44 | Sandy clay loam |
| | 0.45 | 2.51 | 0.03 | 0.17 | 0.34 | 20 | 49 | Clay loam |
| | 2.51 | 3.86 | 0.12 | 0.23 | 0.34 | 12.2 | 45 | Sandy clay loam |
| RG82 (Hydra) | 0 | 0.12 | 1.20 | 2.41 | 3.62 | 7.1 | 33 | Gravelly fine sandy loam |
| | 0.12 | 2.26 | 0.12 | 0.23 | 0.34 | 13.8 | 36 | Gravelly sandy clay loam |
| | 2.26 | 3.86 | 1.20 | 2.41 | 3.62 | 7.8 | 39 | Sandy loam |

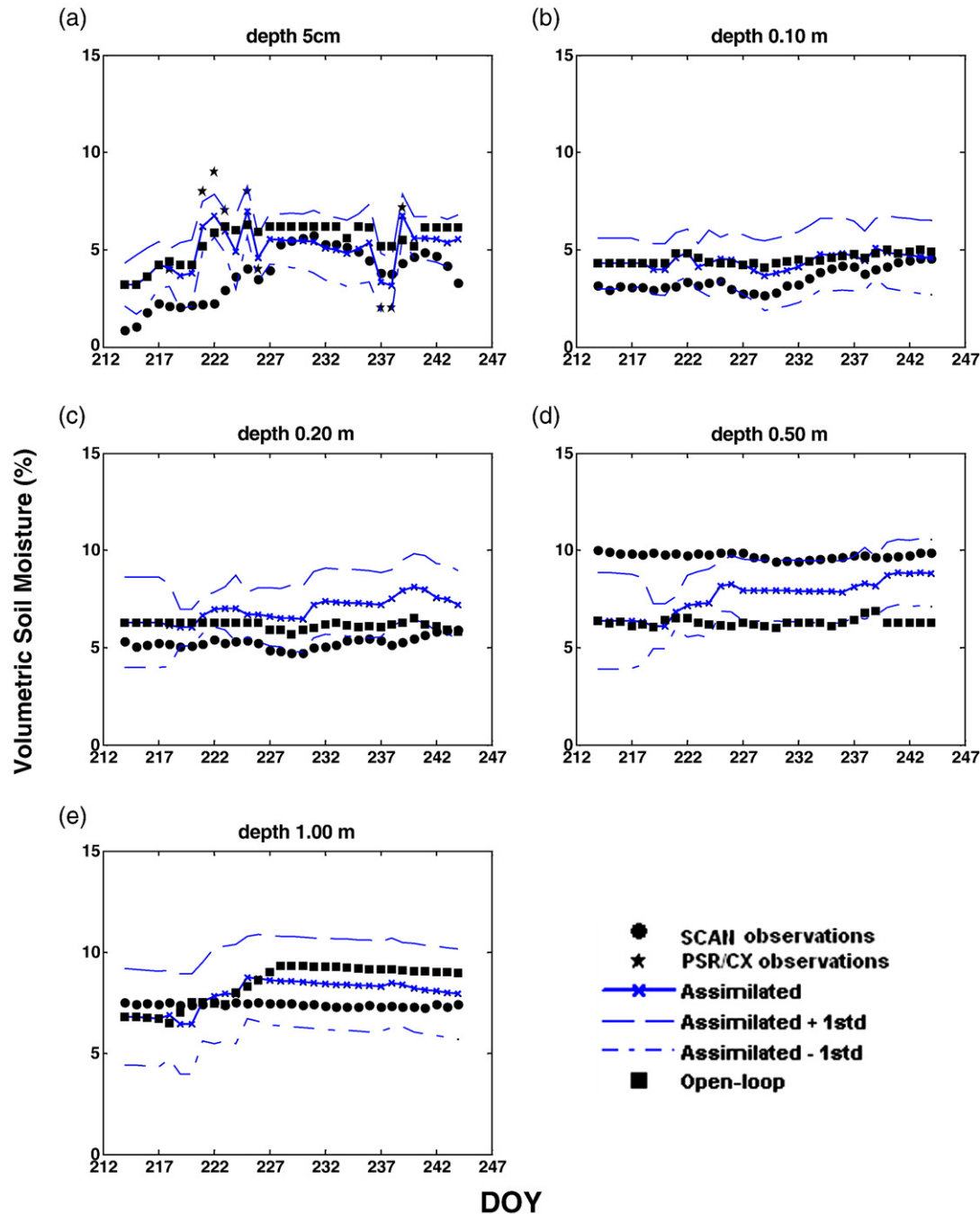


Fig. 9. Comparison of SCAN soil moisture observations with model (with assimilation) simulated soil moisture at depth of (a) 0.05 m, (b) 0.10 m, (c) 0.20 m, (d) 0.50 m, and (e) 1.00 m of Walnut Gulch Experimental Watershed (WGEW).

diminishing effect when the soil layers are nearly similar. In other words, the results from this site show the benefits of providing better soil layer (textural heterogeneity) information as open loop simulation performs reasonably well. At 0.10 m depth, soil moisture values were constrained due to residual water content of the soil layer. Data assimilation could not improve over open-loop and they are almost similar. Whereas, at 0.20 m depth, soil moisture values are slightly more than the residual water content and data assimilation adjusts the soil moisture and deviate it further from SCAN observations. This effect exhibits another good example of having very gravelly sandy soil and how it

influences the soil moisture observations and data assimilation. It is quite apparent from Fig. 9d–e, that data assimilation did improve the prediction over open-loop.

3.1.2. Hydra Site (RG46)

This rain-gauge site (RG46) is situated in a shrubland at an altitude of 1442 m above the sea level. Fig. 8 shows the amount of precipitation received at this site during the SMEX04 experiment. Hydra soil moisture sensors are installed at 0.13, 0.38, and 0.76 m depths at this site. The top two sensors are in the second soil layer (Table 1: sandy clay loam), and the sensor

at 0.76 m is in the third soil layer (Table 1: clay loam). The states of soil moisture at these depths (Fig. 10a–c) were predominantly influenced by the clay loam (CL) texture of the layers (Table 1). The PSR/CX-based surface soil moisture observations for the pixel at this site are very low, ranging from 2 to 3% by volume, which is much below θ_r for the surface soil used in the modeling. Very low remotely sensed surface soil moisture for the pixel could be attributed to rock fraction on the surface. The effect of PSR/CX data assimilation is clearly visible at the depth of 0.13 m (Fig. 10a). However, the effect of data assimilation diminishes at the deeper depths of 0.38 and 0.76 m (Fig. 10b–c). It is also important to note that starting the model for a month before SMEX04 primed the initial conditions in both the assimilated and open-loop models quite close to the Hydra measurements. For the entire SMEX04 duration, the Hydra measurements for this site were within the bounds of ± 1 SD of the assimilated model predictions.

3.1.3. Hydra Site (RG82)

The RG82 site is at 1518 m above the sea level and located in a shrubland. The site received small amount of precipitation during the SMEX04 period (Fig. 8). As for the other sites, the PSR/CX measurements for this site were influenced by the gravelly sandy loam texture at the soil surface. As illustrated in Fig. 11a PSR/CX measurements are very low (much below θ_r of

soil surface from SSURGO) which was due to overall rock fraction on the soil surface in the pixel. Of the three soil layers considered in modeling this site, the middle layer contained clay (Table 1) that impeded water movement. All the three Hydra soil moisture sensors at the depths 0.13, 0.38, and 0.76 m are installed in the middle soil layer (gravelly sandy clay loam). Fig. 11a–c show very small fluctuations in soil moisture as a result of high retention by the clay content. In the time stability study, Vachaud et al. (1985) described the relation between soil water content and soil texture and demonstrated that locations with the high clay content remain most wet at all times. The assimilated and open-loop models performed equally well in describing the soil moisture trend. Comparisons of Hydra measurements with assimilated and open-loop models show a good agreement at all the three depths and the match improved with depth. At this site the Hydra observations were completely contained within ± 1 SD of the assimilated model predictions.

3.2. Spatio-temporal variability of soil moisture in WGEW

From the results presented above for the three test sites, it is evident that the assimilated model ensembles for a particular pixel reasonably describe the variability present at the respective depths. The averages from these ensembles for 224 different pixels are used to characterize the soil moisture states

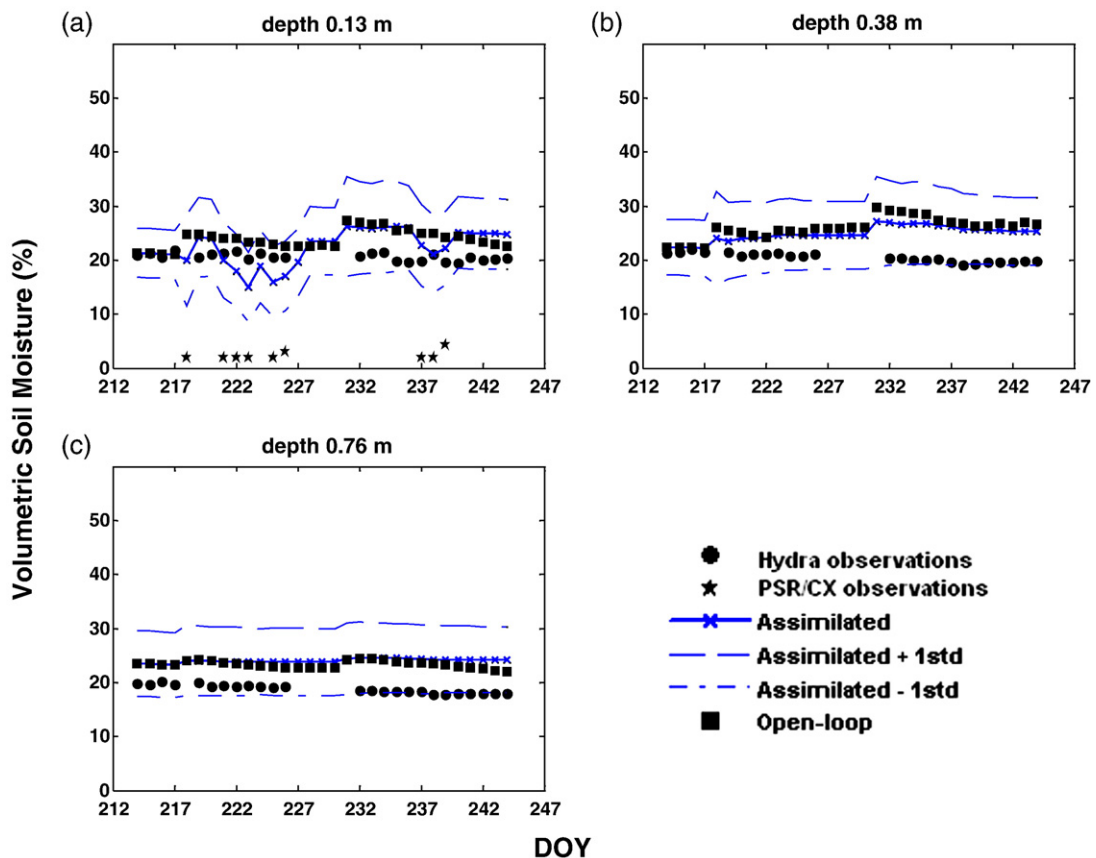


Fig. 10. Comparison of Vitel (RG46) soil moisture observations with model (with assimilation) simulated soil moisture at depth of (a) 0.13 m, (b) 0.38 m, and (c) 0.76 m of Walnut Gulch Experimental Watershed (WGEW).

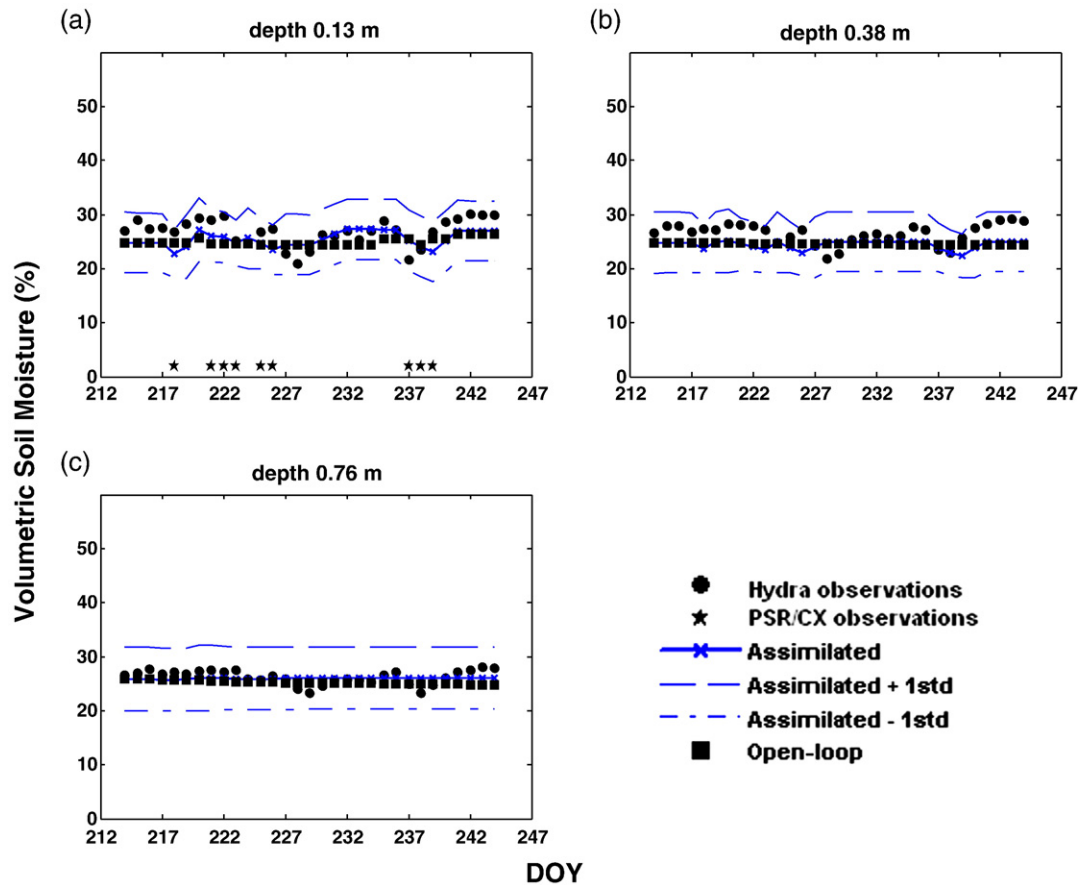


Fig. 11. Comparison of Vitel (RG82) soil moisture observations with model (with assimilation) simulated soil moisture at depth of (a) 0.13 m, (b) 0.38 m, and (c) 0.76 m of Walnut Gulch Experimental Watershed (WGEW).

at various depths across the WGEW (Fig. 12). Western et al. (2002) showed that the normal distribution fits best for spatial representation of soil moisture. A kernel smoothing technique (Silverman, 1981) was used to compute the normal probability density of soil moisture at the depths of 0.01, 0.05, 0.10, 0.20, 0.50, 0.75, 1.00, 1.50, and 3.50 m at the WGEW scale. At each depth 31 (daily) realizations of probability density (Fig. 12) from DOY 214 to 244 (August 1st to August 31st 2004) are presented using 22400 (224 footprints \times 100 ensembles) soil moisture estimates.

Fig. 12a–i reveal the transition of soil moisture probability densities and describe the temporal variability across the soil profiles in the WGEW. For most of the days between DOY 214 to 244, unimodality in soil moisture probability density was observed in the top 0.05 m depth (Fig. 12a–b). Variation in magnitude of the peak densities for 31 days is apparent at the depth of 0.01 m (Fig. 12a). We suggest that the change in the mean and variance of the daily soil moisture probability densities at the 0.01 m depth (Fig. 12a) is due to the highly variable (localized) convective summer precipitation patterns across the WGEW. However, at 0.05 m depth, the variation in soil moisture probability density peaks is less pronounced as compared to the probability density at the 0.01 m depth. Western et al. (2002) found that the bounded normal probability densities of soil moisture become skewed and less variable as

the means approach the lower bound *i.e.*, residual water content. In our study, as the Gaussian kernel estimates at shallow depths (0.01 and 0.05 m, Fig. 12a–b) approach the lower boundary, probability densities become positively skewed with small spread/variation. This behavior is also consistent with the findings of Famiglietti et al. (1999). It is noteworthy that during the SMEX04 period no shift was observed from positively skewed (dry: near lower bounds) to moderate (midrange of wetness) or negatively skewed (wet: near upper bounds) probability densities at 0.01 m and 0.05 m depths. This limited variation in soil moisture skewness indicates an absence of uniform rainfall events over the whole watershed domain as illustrated in Fig. 5. Further, positively skewed narrow densities with little or no variation were attributed to a very conductive (sandy texture) top soil layer and little precipitation at WGEW.

With increasing depth (0.10 m to 3.50 m), realizations with multi-modal kernel density estimates were observed (Fig. 12c–i). Mixture of distinct Gaussian probability density functions (PDFs) was apparent in these multimodal densities. The persistence of these distinct Gaussian PDFs in the multimodal densities was observed at specific soil moisture values. Little difference in mean and variance was observed in the distinct Gaussian PDFs across the DOYs (Fig. 12c–i). Also, multimodality of probability density was much more pronounced for the deeper depths than near the

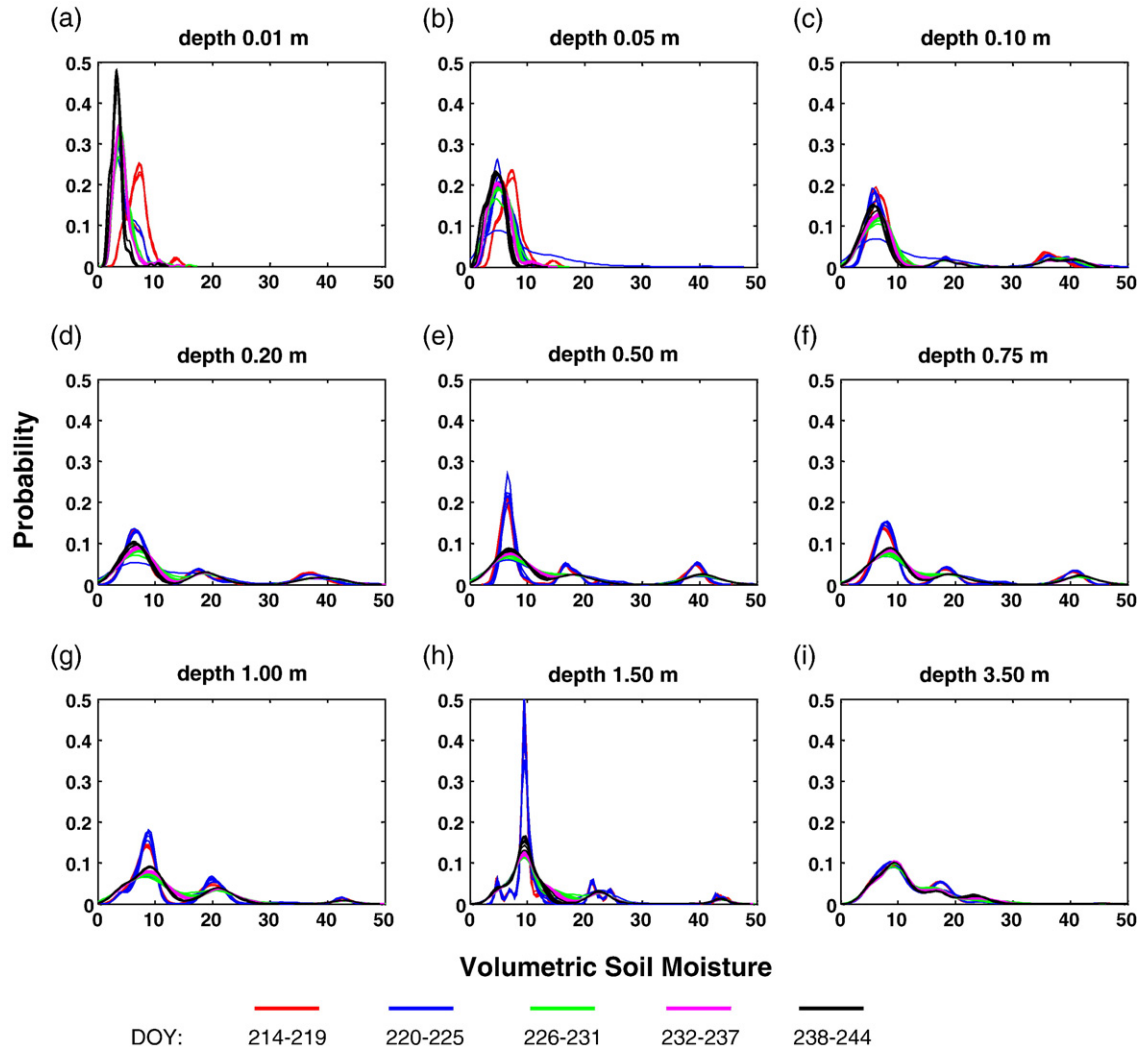


Fig. 12. Walnut Gulch Experimental Watershed (WGEW) soil moisture densities at depth of (a) 0.01 m, (b) 0.05 m, (c) 0.10 m, (d) 0.20 m, (e) 0.50 m, (f) 0.75 m, (g) 1.00 m, (h) 1.50 m, and (i) 3.50 m at resolution of 800 m × 800 m.

soil surface (Fig. 12). A spike in probability distribution was detected at the depth 1.50 m (Fig. 12h). A logical explanation for this spike is internal drainage or redistribution. During redistribution, relatively deeper layer (at 1.50 m) draw soil moisture from the upper layers. It is apparent from Fig. 12e–g, that nominal spikes were also present for DOY 214–225 at the depths of 0.50 m, 0.75 m, and 1.00 m. The time-varying rate of redistribution depends not only on the hydraulic properties of the conducting soil but also on the initial soil moisture status (wetting front depth and the relative dryness of the deeper layers). When the initial wetting front depth is small and the underlying soil is relatively dry, the hydraulic gradient augmenting the gravitational gradient are likely to be strong and hence induce a rapid rate of redistribution.

To understand the spatial variability of soil moisture across the WGEW, *kmean* clustering (Jain & Dubes, 1988) was conducted on 22400 (224 footprints × 100 ensembles) soil moisture estimates at the depths of 0.01, 0.05, 0.10, 0.20, 0.50, 0.75, 1.00, 1.50, and 3.50 m for all 31 days of SMEX04. Table 2 shows the number of spatial clusters of soil moisture at specified

depths in WGEW. Table 2 also provide spatial clustering of texture related soil hydraulic properties *i.e.*, saturated hydraulic conductivity (K_{sat}), residual water content (θ_r), and saturated water content (θ_s) across the WGEW. Number of clusters of θ_r and θ_s are nearly similar at all the specified depths, whereas in

Table 2
Spatial clusters (SC) of soil moisture and hydraulic parameters across WGEW at specified depths

| Soil profile depth in m | Soil moisture SC | Saturated hydraulic conductivity (K_{sat}) SC | Residual water content (θ_r) SC | Saturated water content (θ_s) SC |
|-------------------------|------------------|---|--|---|
| 0.01 | 1 | 4 | 14 | 11 |
| 0.05 | 2 | 4 | 14 | 13 |
| 0.10 | 3 | 7 | 12 | 14 |
| 0.20 | 3 | 8 | 13 | 11 |
| 0.50 | 3 | 9 | 14 | 13 |
| 0.75 | 3 | 9 | 10 | 12 |
| 1.00 | 8 | 10 | 12 | 12 |
| 1.50 | 9 | 10 | 11 | 11 |
| 3.50 | 12 | 10 | 10 | 10 |

case of K_{sat} the number of spatial clusters increases with the depth. The smaller number of K_{sat} spatial clusters (4 clusters for 0.05 m depth) corroborate with the presence of large percentages of rock and gravel fraction on the soil surface. Based on the groupings of saturated hydraulic conductivity and soil moisture spatial clusters, three distinct depth-dependent zones (i) 0–0.05 m, (ii) 0.05–0.75 m, and (iii) below 0.75 m can be identified in the soil profile. The number of clusters in the spatial distributions of soil moisture for the depths of 0.01 m, 0.05 m, and 0.75 m were somewhat matching to the modality in the respective probability distributions in Fig. 12. Also note that a sudden increase in the number of soil moisture spatial clusters was observed below 1.00 m depth. The numbers of spatial clusters found at these deeper depths were close to the number of soil textures encountered at these specific depths. Based on these findings we suggest that soil texture takes control of soil moisture evolution and spatial distribution with increasing depth and with lesser influence from forcings and feedbacks at the land–atmosphere boundary. At the depths between 0.05 and 1.00 m, plant roots play a major role in describing the status of soil moisture. In our SWAP model simulations the maximum rooting depth was prescribed to be 1.00 m. Plant root water uptake is largely controlled by soil water status and spatial (horizontal–vertical) variability of soil moisture. Root–soil interaction tends to equalize soil water content in the root zone. The tendency of homogenization of soil moisture at these depths resulted in three spatial clusters which could be attributed to root dynamics of various vegetation types present in the WGEW. The phenomenon of homogenizing soil moisture in the root zone also reduces soil water flux variability.

Based on the above results it is clear that a coarse spatial resolution of 800 m × 800 m and daily time scale for model simulations influence the evolution of profile soil moisture and other hydrologic responses in WGEW during SMEX04. Furthermore, because of the scanty and scattered nature of rainfall within WGEW during the SMEX04 period and highly conductive nature of the top soil layer, no significant surface runoff and runoff were observed at a coarse resolution of 800 m × 800 m. The topographic control on spatial distribution of soil moisture was not apparent due to sustained dry period. This finding agrees with those of Chang and Islam (2003), where they demonstrated that soil physical properties and topography control spatial variations of soil moisture over large areas. They have shown that topographical control dictates soil moisture distribution under wet conditions, and soil physical properties control variations of soil moisture under drier conditions. Based on these arguments and our results we suggest that at the remote sensing pixel scale the effect of topography and patchy rainfall on the spatio-temporal distribution of soil moisture at the soil surface and deeper depths was not found to be as significant as that of soil texture in the WGEW during SMEX04.

4. Summary and conclusion

The distribution, behavior, and evolution of soil moisture at various depths in the Walnut Gulch Experimental Watershed,

Arizona, during SMEX04 were studied. Aircraft based remotely sensed surface soil moisture for the WGEW was assimilated using EnSRF to model root zone soil moisture up to a depth of 3.86 m. The modeled root zone soil moisture was evaluated with *in situ* measurements from several Hydra and SCAN sites. The comparison shows significant benefits of providing better soil layer/property information, and the propagation of EnSRF Kalman gain through the land surface model SWAP. Reasonable agreement was observed for the shallow depths (0–0.50 m). Most of the measurements at these depths were within ±1 standard deviation of the modeled soil moisture. The models with assimilation and without assimilation (open-loop) performed equally well at deeper depths using soil layer information from the SSURGO database. The results also demonstrated the impact of data assimilation of PSR/CX-based surface soil moisture measurements reaching deeper layers having similar hydraulic properties. In case of the presence of deeper soil layers (with different hydraulic properties from the surface soil layer) the propagation of information during data assimilation from the soil surface to deeper layers was found to be ineffective. The ensembles from the PSR/CX-assimilated model output were used for characterizing the probability densities of soil moisture at several depths. The soil moisture probability densities revealed the temporal evolution across the soil profile in the WGEW. Unimodality in soil moisture densities was observed for the top 0.05 m of soil, whereas multimodality was observed for the deeper soil layers for all 31 days of SMEX04. Multimodality in probability density became more pronounced with depth across the soil profile. Almost no appreciable temporal variation in soil moisture probability densities were observed at any depth between 0.01 and 3.50 m. An increase in the number of soil moisture spatial clusters with depth was found and could be related to the number of soil textures encountered at the deeper depths (below 1.00 m). An increase in soil moisture spatial clusters suggests that soil texture took control of space-time evolution with increasing depth, while the impact of land–atmosphere interaction diminished. With a coarser resolution of 800 m × 800 m and a temporal resolution of one day, the effect of existing conditions of geophysical factors (*e.g.*, topography, rainfall) on the distribution of soil moisture at deeper depths were found to be less significant in the WGEW during SMEX04.

Further investigation is warranted involving different data assimilation schemes and how they affect the evolution of root zone soil moisture with the use of single layer as opposed to multilayer soil information in different hydroclimatic conditions. Besides, we need to develop an improved modeling/assimilation framework to accommodate higher spatial and temporal resolutions to study diurnal variations in precipitation and other meteorological forcings (*e.g.*, air temperature, wind speed) which may be present at the study site.

Acknowledgements

We would like to acknowledge the partial support of NASA (grant #35410) and NSF (CMG/DMS grant) for this work.

References

- Bindlish, R., Jackson, T. J., Gasiewski, A., Stankov, B., Klein, M., Cosh, M. H., Mladenova, I., Watts, C., Vivoni, E., Lakshmi, V., Bolten, J., & Keefer, T. (2008). Aircraft based soil moisture retrievals under mixed vegetation and topographic conditions. *Remote Sensing of Environment*, 112, 375–390 (this issue).
- Burgers, G., van Leeuwen, P. J., & Evensen, G. (1998). Analysis scheme in the ensemble Kalman filter. *Monthly Weather Bulletin*, 126, 1719–1724.
- Carsel, R. F., & Parrish, R. S. (1988). Developing joint probability distributions of soil water retention characteristics. *Water Resources Research*, 24, 755–769.
- Chang, D. H., & Islam, S. (2003). Effects of topography, soil properties and mean soil moisture on the spatial distribution of soil moisture: A stochastic analysis. In Y. Pachepsky, D. E. Radcliffe, & H. M. Selim (Eds.), *Scaling Methods in Soil Physics* (pp. 193–225). Boca Raton, FL: CRC Press.
- Crosson, W. L., Laymon, C. A., Inguva, R., & Schamschula, M. P. (2002). Assimilating remote sensed data in a surface flux-soil moisture model. *Hydrological Processes*, 16, 1645–1662.
- Crow, W. T., & Wood, E. F. (2003). The assimilation of remotely sensed soil brightness temperature imagery into a land surface model using ensemble Kalman filtering: A case study based on ESTAR measurements during SGP97. *Advances in Water Resources Research*, 26, 137–149.
- Das, N. N., & Mohanty, B. P. (2006). Root zone soil moisture assessment using passive microwave remote sensing and vadose zone modeling. *Vadose Zone Journal*, 5, 296–307.
- Dunne, S., & Entekhabi, D. (2005). An ensemble-based reanalysis approach to land data assimilation. *Water Resources Research*, 41. doi:10.1029/2004
- Engman, E. T., & Gurney, R. J. (1991). *Remote sensing in hydrology*. London, UK: Chapman and Hall.
- Entekhabi, D., Nakamura, H., & Njoku, E. G. (1994). Solving the inverse problem for soil moisture and temperature profiles by sequential assimilation of multifrequency remotely sensed observations. *IEEE Transactions on Geoscience and Remote Sensing*, 32, 438–448.
- Evensen, G. (2003). The ensemble Kalman filter: Theoretical formulation and practical implementation. *Ocean Dynamics*, 53, 343–367.
- Famiglietti, J. S., Devereux, J. A., Laymon, C. A., Tsegaye, T., Houser, P. R., Jackson, T. J., et al. (1999). Ground-based investigation of soil moisture variability within remote sensing footprints during the Southern Great Plains 1997 (SGP97) Hydrology Experiment. *Water Resources Research*, 35(6), 1839–1851.
- Feddes, R. A., Kowalik, P. J., & Zaradny, H. (1978). *Simulation of Field Water Use and Crop Yield*. New York, NY: John Wiley and Sons.
- Houser, P. R., Shuttleworth, W. J., Famiglietti, J. S., Gupta, H. V., Syed, K. H., & Goodrich, D. C. (1998). Integration of soil moisture remote sensing and hydrologic modeling using data assimilation. *Water Resources Research*, 34(12), 3405–3420.
- Houtekamer, P. L., & Mitchell, H. L. (1998). Data assimilation using an ensemble Kalman filter technique. *Monthly Weather Review*, 126, 796–811.
- Ines, A. V. M., & Honda, K. (2005). On quantifying agricultural and water management practices from low spatial resolution RS data using genetic algorithm: A numerical study for mixed-pixel environment. *Advances in Water Resources*, 28, 856–870.
- Jackson, T. J. (1993). Measuring surface soil moisture using passive microwave remote sensing. *Hydrological Processes*, 7, 139–152.
- Jackson, T. J., Le Vine, D. M., Hsu, A. Y., Oldak, A., Starks, P. J., Swift, C. T., et al. (1999). Soil moisture mapping at regional scales using microwave radiometry: The Southern Great Plains hydrology experiment. *IEEE Transactions on Geoscience and Remote Sensing*, 37, 2136–2151.
- Jackson, T. J., & Schmugge, T. J. (1989). Passive microwave remote sensing system for soil moisture: Some supporting research. *IEEE Transactions on Geoscience and Remote Sensing*, GE-27, 35–46.
- Jain, A. K., & Dubes, R. C. (1988). *Algorithms for clustering data*. Prentice-Hall advanced reference series. Upper Saddle River, NJ: Prentice-Hall, Inc.
- Kostov, K. G., & Jackson, T. J. (1993). Estimating profile soil moisture from surface layer measurement—A review. *SPIE*, 1941, 125–136.
- Mantoglou, A. (1992). A theoretical approach for modeling unsaturated flow in the spatially variable soil: effective flow model in finite domains and nonstationarity. *Water Resources Research*, 28(1), 251–267.
- Margulis, S. A., McLaughlin, D., Entekhabi, D., & Dunne, S. (2002). Land data assimilation and estimation of soil moisture using measurements from the Southern Great Plains 1997 Field Experiment. *Water Resources Research*, 38(12), 1299–1317.
- Mitchell, H. L., & Houtekamer, P. L. (2000). An adaptive ensemble Kalman filter. *Monthly Weather Review*, 128, 416–433.
- Monteith, J. L. (1965). Evaporation and environment. *Proceedings of the 19th Symposium of the society for Experimental Biology* (pp. 205–233). New York, NY: Cambridge University Press.
- Njoku, E. G., & Entekhabi, D. (1995). Passive remote sensing of soil moisture. *Journal of Hydrology*, 184(1), 101–130.
- Piepmeyer, J. R., & Gasiewski, A. J. (2001). High-resolution passive microwave polarimetric mapping of ocean surface wind vector fields. *IEEE Transactions on Geoscience and Remote Sensing*, 39, 606–622.
- Reichle, R., McLaughlin, D., & Entekhabi, D. (2002). Hydrologic data assimilation with the ensemble Kalman filter. *Monthly Weather Review*, 130(1), 103–114.
- Schmugge, T. J., Gloersen, P., Wilheit, T., & Geiger, F. (1974). Remote sensing of soil moisture with microwave radiometers. *Soil Science Society of American Proceedings*, 28, 721–724.
- Schmugge, T. J., Jackson, T. J., & McKim, H. L. (1980). Survey of methods for soil moisture determination. *Water Resources Bulletin*, 16, 961–979.
- Schmugge, T. J., Meeneely, J. M., Rango, A., & Neff, R. (1977). Satellite microwave observations of soil moisture variations. *Water Resources Bulletin*, 13, 265–286.
- Silverman, B. W. (1981). Using kernel density estimate to investigate multimodality. *Journal of the Royal Statistical Society. Series B*, 43, 97–99.
- Vachaud, G., De Silans, A. P., Balabanis, P., & Vauclin, M. (1985). Temporal stability of spatially measured soil water probability density function. *Soil Science Society of America Journal*, 49, 822–828.
- Van Dam J. C., Huygen, J., Wesseling, J. G., Feddes, R. A., Kabat, P., Van Walsum, P. E. V. (1997). Theory of SWAP version 2.0: Simulation of water and plant growth in the soil–water–atmosphere–plant environment. Technical Document 45. Wageningen Agricultural University and DLO Winand Staring Centre, The Netherlands.
- Western, A. W., Grayson, R. B., & Blöschl, G. (2002). Scaling of soil moisture: A hydrologic perspective. *Annual Review of Earth and Planetary Sciences*, 30, 149–180.
- Whitaker, J. S., & Hamill, T. M. (2002). Ensemble data assimilation without perturbed observations. *Monthly Weather Review*, 130, 1913–1924.
- Wie, M. Y. (1995). *Soil moisture: Report of a workshop held in Tilburon, California*. NASA Conf. Publ. CP-3319.
- Zhang, D. X. (1999). Nonstationary stochastic analysis of the transient unsaturated flow in randomly heterogeneous media. *Water Resources Research*, 35(4), 1127–1141.